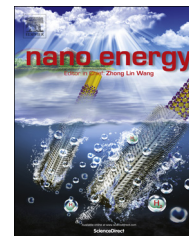




Available online at [www.sciencedirect.com](http://www.sciencedirect.com)

ScienceDirect

journal homepage: [www.elsevier.com/locate/nanoenergy](http://www.elsevier.com/locate/nanoenergy)



RAPID COMMUNICATION

# Graphene decorated vanadium oxide nanowire aerogel for long-cycle-life magnesium battery cathodes



Qinyou An<sup>a</sup>, Yifei Li<sup>a</sup>, Hyun Deog Yoo<sup>a</sup>, Shuo Chen<sup>b,c</sup>, Qiang Ru<sup>a</sup>,  
Liqiang Mai<sup>d,\*</sup>, Yan Yao<sup>a,c,\*</sup>

<sup>a</sup>Department of Electrical and Computer Engineering & Materials Science and Engineering Program, University of Houston, Houston, TX 77204, USA

<sup>b</sup>Department of Physics, University of Houston, Houston, TX 77204, USA

<sup>c</sup>Texas Center for Superconductivity at University of Houston, Houston, TX 77204, USA

<sup>d</sup>State Key Laboratory of Advanced Technology for Materials Synthesis and Processing, Wuhan University of Technology, Wuhan 430070, China

Received 14 September 2015; received in revised form 18 October 2015; accepted 26 October 2015  
Available online 10 November 2015

## KEYWORDS

Mg-ion batteries;  
Shielding effect;  
Vanadium oxide;  
Graphene;  
Aerogel

## Abstract

We report graphene decorated hydrated vanadium oxide nanocomposite as an effective cathode material for long cycle-life Mg storage. Excellent electrochemical performance with specific capacity of 330 mAh g<sup>-1</sup> at low rate and stable cycling of 200 cycles with 81% capacity retention at 1 A g<sup>-1</sup> was reported. Furthermore, the nanocomposite cathode shows a broad working temperature window from -30 °C to 55 °C with over 200 mAh g<sup>-1</sup> capacity at 55 °C (1.0 A g<sup>-1</sup>). The charge shielding effect of crystal water in the aerogel enhances the Mg<sup>2+</sup> insertion kinetics and the porous structure of aerogel allows easy access of electrolyte into the active material. The cycling performance, rate performance and broad temperature adaptability demonstrate that the graphene decorated vanadium oxide nanowire aerogel is a promising and attractive cathode material for practical Mg batteries.

Published by Elsevier Ltd.

\*Corresponding authors.

E-mail addresses: [mlq518@whut.edu.cn](mailto:mlq518@whut.edu.cn) (L. Mai), [yao4@uh.edu](mailto:yao4@uh.edu) (Y. Yao).

## Introduction

Developing low-cost and safe batteries for electric vehicles and grid scale energy storage has become increasingly the focus of battery research [1–5]. Rechargeable magnesium ion batteries (MIBs) have emerged as an attractive candidate due to the unique advantages of Mg metal, such as high abundance, safe to handle, low standard electrode potential and high volumetric capacity ( $3837 \text{ mAh cm}^{-3}$ ) [6–9]. Since Aurbach's pioneering work in 2000 [10], significant progresses have been witnessed in the quest for better MIB, including the development of cathode materials [11–18], electrolytes [19–22], and anode materials [23, 24]. One major obstacle that restricts the development of MIBs is the difficulty to find a high voltage Mg cathode material with decent Mg intercalation kinetics originated from the strong polarizing nature of divalent Mg ions. [6] This challenge is further exacerbated due to the lack of non-nucleophilic, non-corrosive electrolytes with wide electrochemical window compatible with cathode materials [22]. Our previous work demonstrated a controlled interlayer expansion approach, which boosts Mg diffusivity by two orders of magnitude and effectively enabling the otherwise barely active  $\text{MoS}_2$  to approach its theoretical storage capacity [25]. However, due to the nature of chalcogenides, the redox potential is lower than 2 V vs.  $\text{Mg}/\text{Mg}^{2+}$  and needs to be further increased [26]. Thus, we turned to vanadium pentoxide ( $\text{V}_2\text{O}_5$ ), a well-known high voltage cathode material in lithium-ion batteries [27,28] in search for higher voltage Mg cathodes.

$\text{V}_2\text{O}_5$  has attracted people's attention as a potential candidate for Mg cathodes in 1993 when P. Novak et al. first demonstrated that the insertion kinetics and specific capacity of  $\text{Mg}^{2+}$  could be drastically enhanced when 1 M  $\text{H}_2\text{O}$  was added into the  $\text{Mg}(\text{ClO}_4)_2$  acetonitrile electrolyte [29]. The enhancement is due to the charge shielding effect of dipole molecule ( $\text{H}_2\text{O}$ ) that transformed  $\text{Mg}^{2+}$  into less polarizing solvated ions (Figure 1a). To prevent undesirable water reaction with the anode, the researchers further used insertion hosts that already contain water in their crystal structure [30]. However, rapid capacity fading occurred due to water ejection from the crystal structure of the host. Recently, E.S. Takeuchi et al. reported the synthesis of hydrated magnesium vanadium oxide ( $\text{Mg}_{0.1}\text{V}_2\text{O}_5 \cdot 1.8\text{H}_2\text{O}$ ) using a novel sol gel method [31]. Similarly, crystal water molecules in the structure coordinate to  $\text{Mg}^{2+}$  as the solvation shell to effectively screen the divalent charge. Discharge capacity of  $280 \text{ mAh g}^{-1}$  has been reported, however, cycling was only limited to 7 cycles. Therefore, substantial advances are required for the development of cathode materials with higher capacity, better cycling stability and excellent rate capability.

Here we report the synthesis of hydrated vanadium oxide nanowire/graphene nanocomposites (VOG-1) prepared via a facile reaction and subsequent freeze-drying process. The nanowire/graphene nanocomposite features both rapid electron transport and  $\text{Mg}^{2+}$  diffusion due to the small diameter of nanowires, large surface area and excellent structure stability (Figure 1b). The nanocomposites displayed outstanding electrochemical performance: high capacity ( $\sim 330 \text{ mAh g}^{-1}$ ), high-rate cycling stability (80% capacity retention for 200 cycles) and broad working temperature range ( $-30^\circ\text{C}$  to  $55^\circ\text{C}$ ). The excellent electrochemical performance provides

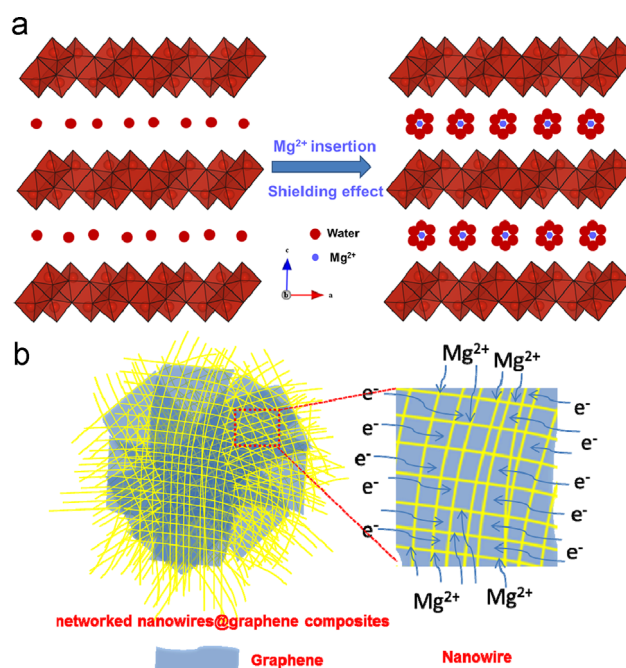


**Figure 1** (a) Shielding effect of  $\text{Mg}^{2+}$  in the hydrated  $\text{V}_2\text{O}_5 \cdot n\text{H}_2\text{O}$ . The strong polarization of the divalent  $\text{Mg}^{2+}$  could be significantly reduced by solvating with crystal water molecules. (b) Schematic illustration of the  $\text{V}_2\text{O}_5 \cdot n\text{H}_2\text{O}@r\text{GO}$  nanocomposite with bi-continuous electron/ion transport pathways, large area of electrode-electrolyte interface, and facile strain relaxation during  $\text{Mg}^{2+}$  insertion/extraction.

new opportunities for developing cathode materials for practical Mg batteries.

## Experimental section

### Materials synthesis

For the synthesis of hydrated vanadium oxide nanowire/graphene nanocomposites (VOG-1), the pre-prepared  $\text{V}_2\text{O}_5$  sol (20 mL, 0.05 M) and rGO suspension (20 mL,  $\sim 0.5 \text{ mg mL}^{-1}$ ) were mixed in a 100 ml beaker and stirred at room temperature for 1 h. Next,  $\text{NH}_4\text{H}_2\text{PO}_4$  (3.0 mmol) was added into the mixture and stirred at  $80^\circ\text{C}$  for 6 h. After aging at room temperature for 2 h, the hydrogels were washed by water several times to remove remaining  $\text{NH}_4\text{H}_2\text{PO}_4$ . Subsequently, the as-prepared hydrogels were frozen and freeze-dried to partially remove  $\text{H}_2\text{O}$ . Elemental analysis shows the graphene accounts for 3.4% of total weight of VOG-1. In comparison, VOG-2 sample was prepared by annealing VOG-1 at  $350^\circ\text{C}$  for 2 h in argon atmosphere. VOG-3 sample was prepared by annealing VOG-1 at  $350^\circ\text{C}$  for 2 h in air to convert to crystalline  $\text{V}_2\text{O}_5$ . See the supporting information for the synthesis details of rGO and  $\text{V}_2\text{O}_5$  sols.

### Materials characterizations

The samples were characterized by XRD (Rigaku MiniFlex 600) using  $\text{Cu K}\alpha$  radiation ( $\lambda = 1.5406 \text{ \AA}$ ), X-ray photoelectron spectroscopy (XPS, VG MultiLab 2000), thermogravimetric

analysis (TA instruments Q50), physisorption analysis (Micromeritics Tristar II 3020 plus) using N<sub>2</sub>, scanning electron microscopy (SEM; Gemini LEO 1525), and transmission electron microscopy (TEM, JEM-2100F).

### Electrochemical characterizations

The electrochemical performance was measured with three-electrode cells assembled in an Ar-filled glove box. The working electrode is made of a mixture of active materials (60 wt%), acetylene black (30 wt%), and poly(tetrafluoroethylene) (PTFE, 10 wt%) with a mass loading of  $\sim 1 \text{ mg cm}^{-2}$  on stainless steel meshes. Activated carbon (AC) clothes (Fuel Cell Earth LLC) were used as both counter electrode and quasi-reference electrode. A solution of 0.5 M magnesium bis(trifluoromethane sulfonyl) imide ( $\text{Mg}(\text{TFSI})_2$ ) in acetonitrile was used as the electrolyte. The potential of AC cloth was measured to be 0.12 V vs. ferrocene/ferrocenium, i.e. 2.4 V vs.  $\text{Mg}/\text{Mg}^{2+}$  [32]. The working electrodes

were operated within  $-0.8$  and  $1.0$  V vs. AC, equivalent to  $1.6$  and  $3.4$  V vs.  $\text{Mg}^{2+}/\text{Mg}$ . Galvanostatic charge/discharge cycling, cyclic voltammetry and electrochemical impedance spectroscopy were measured using a potentiostat (Bio-Logic VMP-3). The temperature dependent experiment was conducted in an environmental chamber (Tenny TJR-A-WF4, temperature range  $-73$  to  $200$  °C).

### Results and discussion

Figure 2a illustrates the fabrication process of VOG-1 nanocomposites.  $\text{V}_2\text{O}_5$  sol and rGO were prepared following literatures separately [33, 34], both of which are negatively charged. Then they were mixed under stirring while  $\text{NH}_4\text{H}_2\text{PO}_4$  was added to contribute positive charges. Graphene and  $\text{V}_2\text{O}_5$  sols self-assembled due to the electrostatic interactions. The vanadium oxides gel grew into continuous vanadium oxide nanowires due to Ostwald ripening, which subsequently integrated as hydrated vanadium oxide@rGO

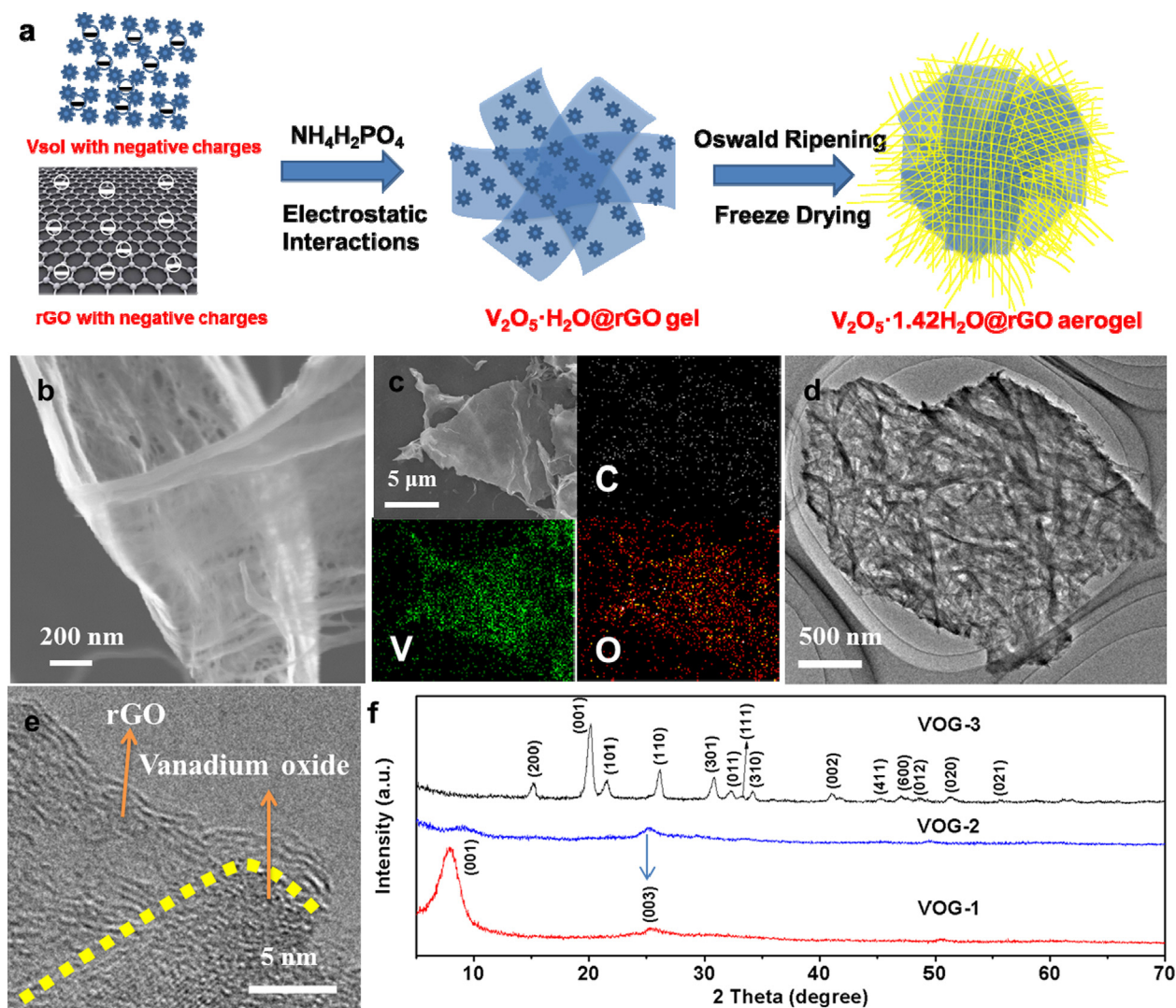


**Figure 2** (a) Schematic illustration of the fabrication process and proposed formation mechanism of the  $\text{V}_2\text{O}_5 \cdot 1.42\text{H}_2\text{O}@r\text{GO}$  aerogel (VOG-1). (b) SEM image, (c) elemental mapping images, (d-e) TEM images of the VOG-1. (f) The XRD patterns of VOG-1, VOG-2 and VOG-3. VOG-2 and VOG-3 were prepared by annealing VOG-1 at  $350$  °C in argon and air, respectively. The VOG-1 composite displays a large interlayer spacing of  $\sim 11.3$  Å.

nanocomposites via the freeze-drying process. The morphology and structure of as-prepared VOG-1 were investigated by SEM and TEM. As shown in Figure 2b, the highly interconnected and porous three dimensional (3D) nanocomposites are built from numerous graphene nanosheets and vanadium oxide nanowires (Figure S1-S2). The diameters of vanadium oxide nanowires range from 10 nm to 20 nm. To confirm its composition, as-prepared VOG-1 was studied by energy dispersive X-ray spectroscopy (EDX). As shown in Figure 2c, the V, O and C atoms are homogeneously distributed in the composite. Furthermore, the TEM image in Figure 2d shows that vanadium oxide nanowires uniformly anchored onto graphene nanosheets. The TEM image (Figure 2e) reveals a few graphene layers located near the edge of the vanadium oxide nanowires.

The water content of the VOG-1 gel was measured by TGA, showing a 12.3% weight loss due to the removal of crystal water (Figure S3). The composition is thus determined as  $V_2O_5 \cdot 1.42H_2O$ . The (001) peak in Figure 2f shows the VOG-1 nanocomposite with large interlayer spacing ( $\sim 11.3 \text{ \AA}$ ), which is common for an aerogel [35]. To study the effect of water content on  $Mg^{2+}$  capacity, VOG-1 sample was annealed at  $350 \text{ }^\circ\text{C}$  for two hours in argon (VOG-2, Figure 2f and S4a). The XRD patterns show broader peaks with lower intensity, suggesting a decrease in crystallinity after thermal treatment. It is noteworthy that even with thermal treatment at  $350 \text{ }^\circ\text{C}$  in argon, the  $V_2O_5$  lamellar structure is still preserved because of remaining water molecules involved in the formation of the polyoxovanadate network [34]. In comparison, when VOG-1 sample was treated at  $350 \text{ }^\circ\text{C}$  in air for two hours (VOG-3, Figure S4b), the aerogel converted to crystalline  $V_2O_5$  phase (Figure 2f). The shift of diffraction peak to higher angle indicates a gradual decrease of interlayer spacing due to the removal of crystal water [35]. Nitrogen adsorption-desorption isotherms were further measured to characterize the porous

structure of the products. The Brunauer-Emmerr-Teller (BET) surface area of VOG-1 is  $28.5 \text{ m}^2 \text{ g}^{-1}$ . The nitrogen adsorption-desorption isotherm of VOG-1 (Figure S5a) appears to be type IV curve with the H3 hysteresis loops that can be linked to slit-shaped pores. The Barrett-Joyner-Halenda (BJH) pore-size distribution curve (inset of Figure S5a) displays the pore sizes in VOG-1 range from 2-4 nm to 20-40 nm. The Raman spectrum of the VOG-1 (Figure S5b) displays two typical peaks of graphene with the D band at around  $1338 \text{ cm}^{-1}$  and G band at around  $1611 \text{ cm}^{-1}$  [36, 37]. Furthermore, XPS result shows that the  $V^{4+}/V^{5+}$  ratio is 14.2% in VOG-1 (Figure S6). The small fraction of  $V^{4+}$  is due to the reduction between molten  $V_2O_5$  and cold water during the preparation of the vanadium oxide sols.

The electrochemical performances of three samples (VOG 1-3) were investigated in a three-electrode tube cell using a  $0.5 \text{ M Mg(TFSI)}_2$  acetonitrile ( $CH_3CN$ ) electrolyte. Although the  $Mg(TFSI)_2$ - $CH_3CN$  electrolyte does not enable reversible Mg deposition/dissolution, it has been found compatible with high voltage oxide cathodes [32]. Activated carbon clothes were used as quasi-reference electrodes, which are known to be stable in  $CH_3CN$ -based electrolyte with potential calibrated as  $2.4 \text{ V vs. Mg}^{2+}/Mg$  [32]. Figure 3a shows the cyclic voltammetry (CV) of VOG-1 composite electrode between 1.6 and  $3.4 \text{ V vs. Mg/Mg}^{2+}$  at a scan rate of  $0.1 \text{ mV s}^{-1}$ . It is clear that the CV curve of the first cycle is quite different from the subsequent cycles, especially in the anodic branch. The cathodic peaks do not change substantially during cycling. But the intensity keeps increasing, revealing higher capacity. Figure 3b displays the typical galvanostatic discharge/charge curves of the three samples at the current density of  $100 \text{ mA g}^{-1}$  with no obvious plateaus observed. Interestingly, VOG-1 exhibits the highest reversible capacity  $\sim 280 \text{ mAh g}^{-1}$  among three samples. Figure 3c shows the cycling stability of at a current density of  $100 \text{ mA g}^{-1}$ . The capacity of VOG-1 increased from 210 to

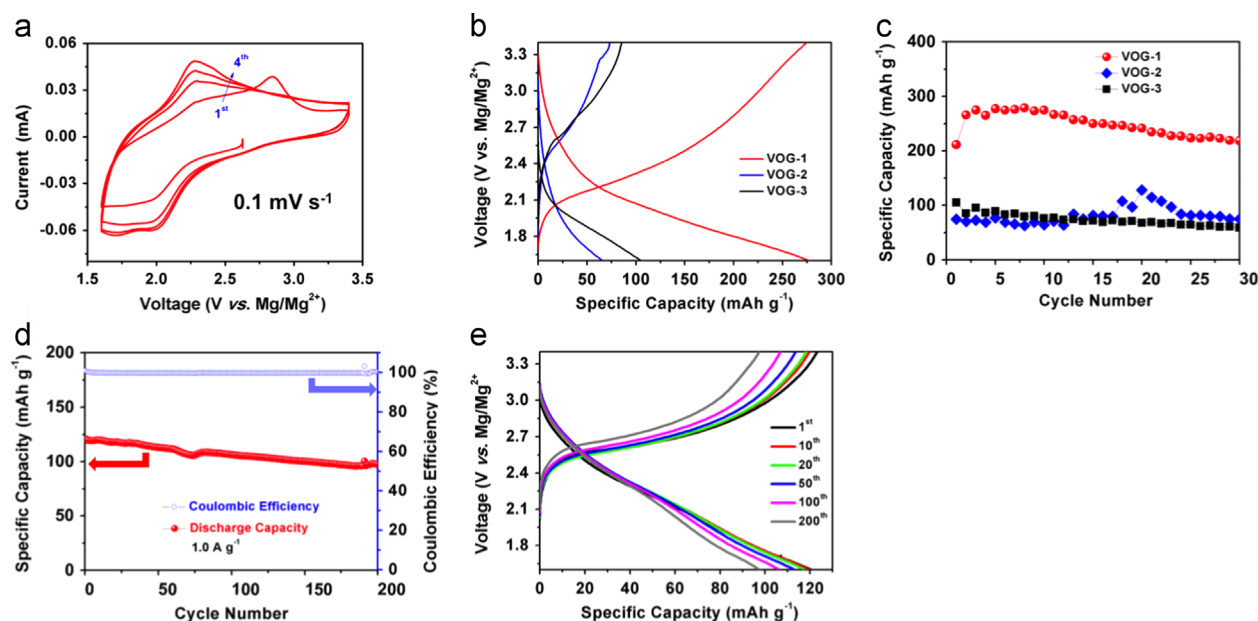


**Figure 3** (a) Cyclic voltammogram of VOG-1 electrode between 1.6 and  $3.4 \text{ V vs. Mg/Mg}^{2+}$  at a scan rate of  $0.1 \text{ mV s}^{-1}$ . (b) Galvanostatic charge-discharge profiles and (c) cycling performance of VOG-1, VOG-2 and VOG-3 at  $100 \text{ mA g}^{-1}$  for Mg storage. (d) Cycling performance and (e) charge-discharge profiles of VOG-1 at  $1.0 \text{ A g}^{-1}$ . The capacity retention is 81% for 200 cycles.

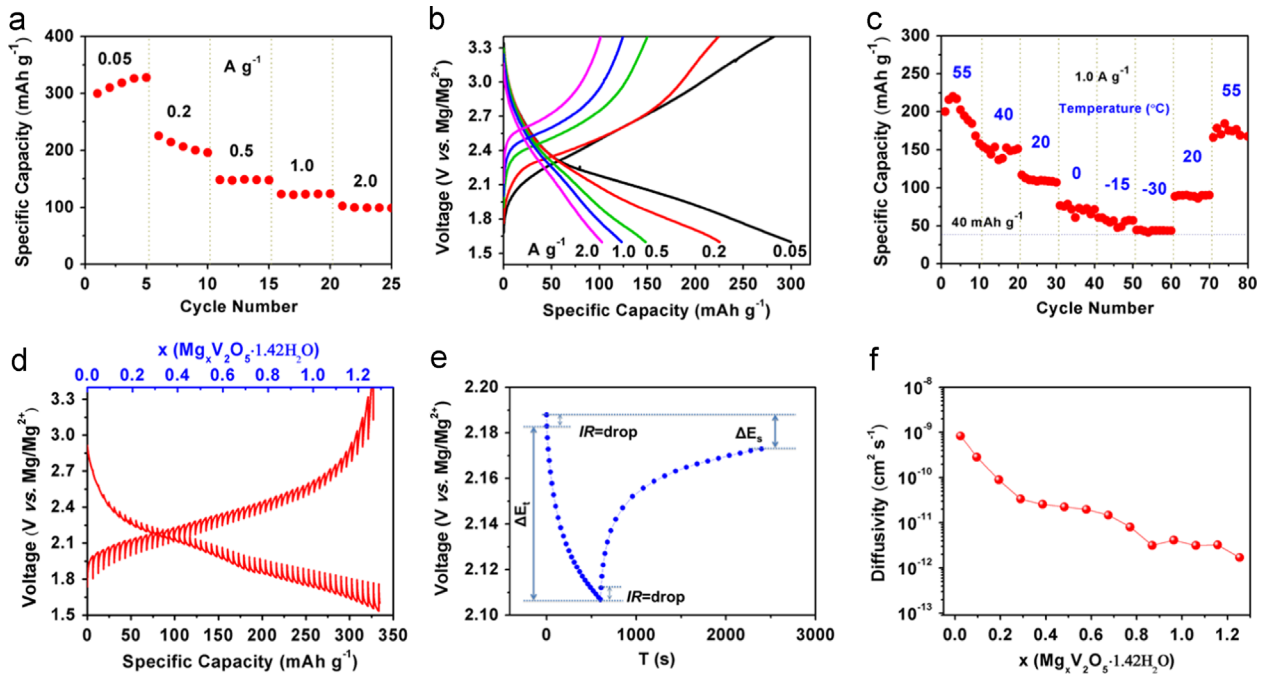


**Figure 4** (a) Rate performance and (b) charge-discharge profiles at various current density. (c) Discharge capacity at various temperatures from  $-30$  to  $55$  °C at  $1.0$  A  $g^{-1}$ . (d) GITT curves, (e) GITT potential response curve with time. The experiment was carried out at constant current pulse of  $20$  mA  $g^{-1}$  for  $10$  min followed by a relaxation period of  $30$  min. (f) Diffusivity versus state of discharge.

$280$  mAh/g in the first three cycles, which is consistent with the observed increasing peak area in CV curves (Figure 3a). In addition to the highest capacity, VOG-1 also exhibits excellent cycling stability (Figure 3d). After  $200$  charge/discharge cycles at  $1.0$  A  $g^{-1}$ , the specific capacity still retains  $81\%$  of the initial value. Remarkably, the coulombic efficiency maintains higher than  $99\%$  during the entire cycles. No obvious change in galvanostatic voltage profiles during the long-term cycling (Figure 3e), demonstrating the excellent structure stability of the nanocomposite.

Since VOG-1 shows the highest capacity and cycling stability, we focus our efforts on investigating the rate capability and temperature adaptability of VOG-1. The rate performance of VOG-1 was measured at different current densities from  $0.05$  A  $g^{-1}$  to  $2.0$  A  $g^{-1}$  (Figure 4a and b). The VOG-1 cathode exhibits a high capacity of  $\sim 320$  mAh  $g^{-1}$  at  $0.05$  A  $g^{-1}$ , which to the best of our knowledge represents the highest Mg intercalation capacity ever reported. Even when the current density increases to  $2.0$  A  $g^{-1}$ , the specific capacity still remains  $\sim 100$  mAh  $g^{-1}$ . The effect of temperature on device performance has also been studied (Figure 4c) in an environmental chamber. When the temperature increases to  $55$  °C, a high discharge capacity of  $\sim 200$  mAh  $g^{-1}$  is demonstrated, which is much higher than the capacity of  $120$  mAh  $g^{-1}$  obtained at room temperature. Remarkably, the cell can deliver reversible capacity of  $40$  mAh  $g^{-1}$  at  $-30$  °C. When the temperature was reset to  $55$  °C after  $80$  cycles, the capacity immediately increased back to  $\sim 170$  mAh  $g^{-1}$ . Such a broad range of working temperature has never been reported for Mg batteries previously. The reversible capacity decreases progressively with decreasing temperature, which could be understood due to slower diffusion of  $Mg^{2+}$  at lower temperature.

To scrutinize the origin of high capacity and broad temperature adaptability of VOG-1, the kinetics of  $Mg^{2+}$

solid-state diffusion were studied with galvanostatic intermittent titration technique (GITT) [38]. The GITT method determines ion diffusivity as a function of depth-of-discharge hence can provide insight into the composition-dependent electrode kinetics. As shown in Figure 4d, VOG-1 delivers a specific capacity as high as  $330$  mAh  $g^{-1}$  in the GITT measurement, corresponding to a discharge product of  $Mg_xV_2O_5$  ( $x=1.25$ ). Moreover, the  $Mg^{2+}$  diffusivity  $D^{GITT}$  can be obtained from the potential response to a small constant current pulse ( $20$  mA  $g^{-1}$ ) via the following formula [39]:

$$D^{GITT} = \frac{4}{\pi\tau} \left( \frac{m_B V_M}{M_B S} \right)^2 \left( \frac{\Delta E_S}{\Delta E_\tau} \right)^2 \quad (1)$$

where  $\tau$  is the constant current pulse time,  $m_B$ ,  $V_M$ ,  $S$ , and  $M_B$  are the mass, molar volume, electrode-electrolyte interface area, and molar mass of VOG-1, respectively. In Figure 4e,  $\Delta E_S$  is the voltage difference during the open circuit period, and  $\Delta E_\tau$  is the total change of cell voltage during a constant current pulse excluding the  $IR$  drop. Figure 4f shows the average Mg diffusivity of VOG-1 cathode over the entire intercalation process  $\sim 3 \times 10^{-11}$  cm $^2$  s $^{-1}$ , which is about one order of magnitude higher than that of Chevrel phase  $Mo_6S_8$  ( $2.6 \times 10^{-12}$  cm $^2$  s $^{-1}$ ) [40] and  $peo_2-MoS_2$  ( $4.4 \times 10^{-12}$  cm $^2$  s $^{-1}$ ) [25]. We also noticed that the Mg diffusivity decreases from  $9 \times 10^{-10}$  to  $1 \times 10^{-12}$  cm $^2$  s $^{-1}$  when the Mg concentration increases in the host due to the charge repulsion when Mg ions get too close to each other. [40]

To address the question whether the origin of high Mg diffusivity is due to the effect of crystal water or the effect of increased interlayer spacing, we prepared four vanadium oxide aerogel (VOA) samples with different content of crystal water by thermally treatment at different temperatures. To focus on crystal effect content effect, these samples were prepared

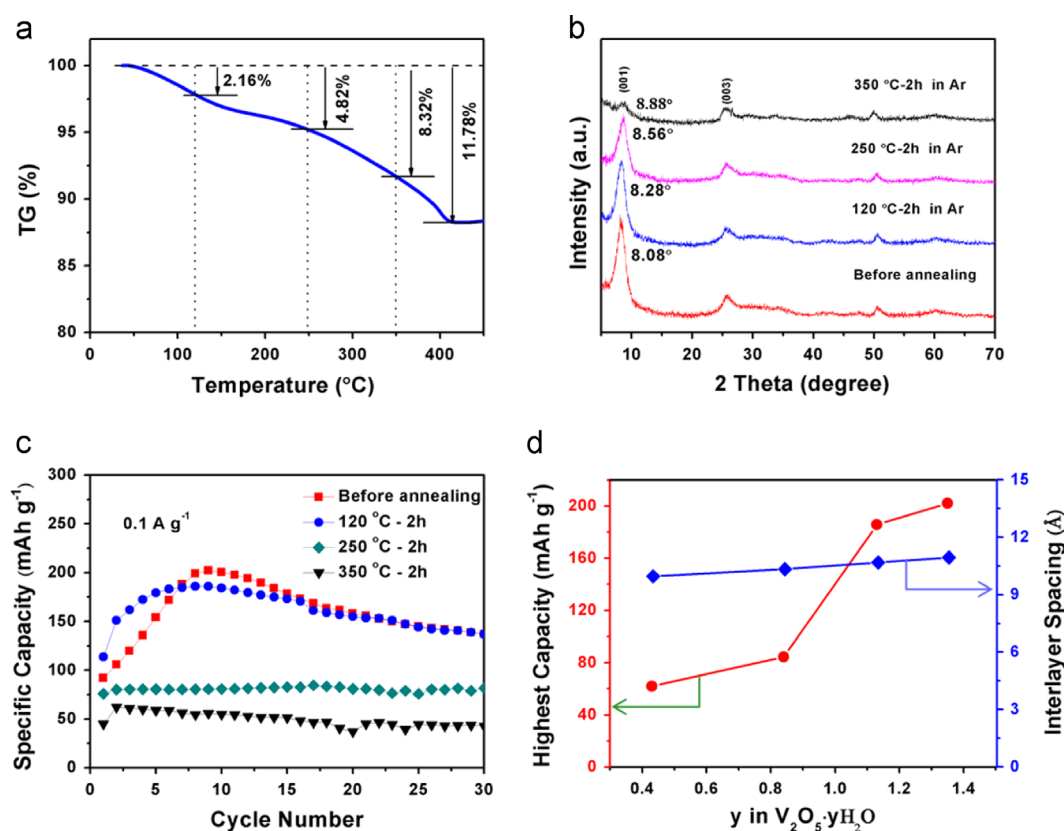


**Figure 5** (a) Thermogravimetric analysis of  $V_2O_5 \cdot 1.35H_2O$ . (b) XRD patterns and (c) cycling performance of samples annealed at different temperatures. (d) The effect of crystal water content on the capacity and interlayer spacing.

without using graphene. TG analysis of the as-made VOA carried out in an argon atmosphere demonstrated the weight loss profile (Figure 5a). As fabricated VOA sample shows the weight loss of 11.78%, corresponding to a formula of  $V_2O_5 \cdot 1.35H_2O$ . For samples annealed at 120 °C, 250 °C and 350 °C for 2 h in argon, their water content are  $V_2O_5 \cdot 1.13H_2O$ ,  $V_2O_5 \cdot 0.84H_2O$  and  $V_2O_5 \cdot 0.43H_2O$ , respectively. Figure 5b shows the (001) peak of hydrated  $V_2O_5$  slightly shifts to higher angles with the decrease of crystal water content, indicating a gradual decrease of the interlayer spacing. Figure 5c compares the electrochemical performance of the four samples cycled at the current density of  $0.1 A g^{-1}$ . Again, the as-fabricated sample shows the highest capacity with an obvious activation stage. The longer activation stage (8 cycles) than that of VOG-1 (3 cycles in Figure 3b) is mainly due to the electrolyte wetting of active materials and the less porous  $V_2O_5$  network when graphene is not used (SEM shown in Figure S7). In other words, the existence of graphene not only increases the conductivity but also improves the dispersibility of the nanocomposite. Going back to the question which effect determines the high Mg capacity, Figure 5d shows that the capacity of  $V_2O_5 \cdot nH_2O$  increases from 60 to 210 mAh/g when  $n$  increases from 0.43 to 1.35. In comparison, the interlayer spacing only increases from 10 to 11 Å. We thus conclude that crystal water plays an important role in shielding the charge of Mg ions to reduce diffusion barrier and increase Mg intercalation capacity. A legitimate concern of water-containing cathode is the negative effect of water to the stability of electrolyte. In this case, since crystal water exists at the interstitial sites of the cathode host, water molecules may not get out of the host easily. For

example, J. Goodenough et al. reported that vacuum-dried  $Na_2MnFe(CN)_6 \cdot 0.3H_2O$  as a high capacity cathode with 75% capacity retention after 500 cycles in Na-ion batteries [41].

Based on above discussions, the superior electrochemical performance of VOG-1 is attributed to the synergetic advantages of crystal water, graphene and fine nanowires as illustrated in Figure 1b. First and foremost, the charge shielding effect from the crystal water molecules between vanadium oxide layers improves the insertion kinetics of  $Mg^{2+}$  ion. The unique nanocomposite architecture of VOG-1 mitigates water ejection from the crystal structure. Second, the conductive graphene decorated vanadium oxide nanowire aerogel offers rapid ion diffusion pathways and efficient electron transport pathways. Third, the porous structure of aerogel increases the interfacial area between electrode and electrolyte, resulting in the excellent rate capability. Finally, the porous aerogel reduces the self-aggregation of active materials and accommodates the volume variation during repeated  $Mg^{2+}$  insertion/extraction, leading to excellent structure stability and cycle life.

## Conclusions

In conclusion, graphene decorated vanadium oxide nanowire aerogels (VOG-1) were synthesized via combining facile precipitation process and freeze-drying method. VOG-1 exhibits so far the best reported Mg storage capacity, remarkable rate capability, and cycling stability. Furthermore, the VOG-1 nanocomposite shows excellent temperature adaptability ( $>200 mAh g^{-1}$  at 55 °C and  $>40 mAh g^{-1}$  at  $-30$  °C). The

excellent electrochemical performance is attributed to the nanocomposite architecture which provides bi-continuous electron/ion pathways, rapid insertion kinetics of  $Mg^{2+}$  ion shielded with crystal water, large electrode-electrolyte interface area and facile strain relaxation. Our work demonstrates the promise of nanostructured electrode design to improve the performance of Mg batteries.

## Acknowledgments

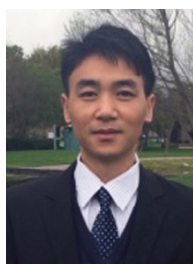
Y.Y. acknowledges the funding support from the U.S. Office of Naval Research (No. N00014-13-1-0543). L. M acknowledges the International Science & Technology Cooperation Program of China (2013DFA50840), the National Science Fund for Distinguished Young Scholars (51425204), and the State Key Laboratory of Advanced Technology for Materials Synthesis and Processing (Wuhan University of Technology, 2014-KF-4).

## Appendix A. Supplementary material

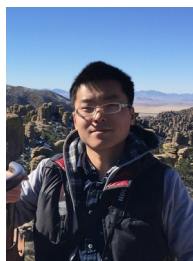
Supplementary data associated with this article can be found in the online version at <http://dx.doi.org/10.1016/j.nanoen.2015.10.029>.

## References

- [1] Z.-S. Wu, G. Zhou, L.-C. Yin, W. Ren, F. Li, H.-M. Cheng, *Nano Energy* 1 (2012) 107-131.
- [2] Y. Yao, F. Wu, *Nano Energy* 17 (2015) 91-103.
- [3] C. Luo, J. Wang, X. Fan, Y. Zhu, F. Han, L. Suo, C. Wang, *Nano Energy* 13 (2015) 537-545.
- [4] X. Wu, Y. Luo, M. Sun, J. Qian, Y. Cao, X. Ai, H. Yang, *Nano Energy* 13 (2015) 117-123.
- [5] F. Wu, J. Qian, R. Chen, T. Zhao, R. Xu, Y. Ye, W. Li, L. Li, J. Lu, K. Amine, *Nano Energy* 12 (2015) 742-749.
- [6] H.D. Yoo, I. Shterenberg, Y. Gofer, G. Gershinsky, N. Pour, D. Aurbach, *Energy Environ. Sci.* 6 (2013) 2265-2279.
- [7] J. Muldoon, C.B. Bucur, T. Gregory, *Chem. Rev.* 114 (2014) 11683-11720.
- [8] H.D. Yoo, Y. Liang, Y. Li, Y. Yao, *ACS Appl. Mater. Interfaces* 7 (2015) 7001-7007.
- [9] Y. Shao, N.N. Rajput, J. Hu, M. Hu, T. Liu, Z. Wei, M. Gu, X. Deng, S. Xu, K.S. Han, J. Wang, Z. Nie, G. Li, K.R. Zavadil, J. Xiao, C. Wang, W.A. Henderson, J.-G. Zhang, Y. Wang, K. T. Mueller, K. Persson, J. Liu, *Nano Energy* 12 (2015) 750-759.
- [10] D. Aurbach, Z. Lu, A. Schechter, Y. Gofer, H. Gizbar, R. Turgeman, Y. Cohen, M. Moshkovich, E. Levi, *Nature* 407 (2000) 724-727.
- [11] N. Pour, Y. Gofer, D.T. Major, D. Aurbach, *J. Am. Chem. Soc.* 133 (2011) 6270-6278.
- [12] N. Wu, Z.Z. Yang, H.R. Yao, Y.X. Yin, L. Gu, Y.G. Guo, *Angew. Chem. Int. Ed.* 54 (2015) 5757-5761.
- [13] C. Kim, P.J. Phillips, B. Key, T. Yi, D. Nordlund, Y.-S. Yu, R. D. Bayliss, S.-D. Han, M. He, Z. Zhang, A.K. Burrell, R.F. Klie, J. Cabana, *Adv. Mater.* 27 (2015) 3377-3384.
- [14] Y.P. Gu, Y. Katsura, T. Yoshino, H. Takagi, K. Taniguchi, *Sci. Rep-Uk* 5 (2015).
- [15] A. Emly, A. Van der Ven, *Inorg. Chem.* 54 (2015) 4394-4402.
- [16] N. Wu, Y.-C. Lyu, R.-J. Xiao, X. Yu, Y.-X. Yin, X.-Q. Yang, H. Li, L. Gu, Y.-G. Guo, *NPG Asia Mater.* 6 (2014) e120.
- [17] Y. Orihara, T. Masese, T. Mori, M. Hattori, K. Yamamoto, T. Okado, Z.-D. Huang, Y. Uchimoto, Y. Koyama, T. Minato, C. Tassel, J. Kim, Y. Kobayashi, T. Abe, H. Kageyama, *Sci. Rep-Uk* 4 (2014) 5622.
- [18] T. Ichitsubo, S. Yagi, R. Nakamura, Y. Ichikawa, S. Okamoto, K. Sugimura, T. Kawaguchi, A. Kitada, M. Oishi, T. Doi, E. Matsubara, *J. Mater. Chem. A* 2 (2014) 14858-14866.
- [19] T. Liu, J.T. Cox, D. Hu, X. Deng, J. Hu, M.Y. Hu, J. Xiao, Y. Shao, K. Tang, J. Liu, *Chem. Commun.* 51 (2015) 2312-2315.
- [20] T. Yamanaka, A. Hayashi, A. Yamauchi, M. Tatsuinisago, *Solid State Ion.* 262 (2014) 601-603.
- [21] T.J. Carter, R. Mohtadi, T.S. Arthur, F. Mizuno, R.G. Zhang, S. Shirai, J.W. Kampf, *Angew. Chem. Int. Ed.* 53 (2014) 3173-3177.
- [22] O. Tutusaus, R. Mohtadi, T.S. Arthur, F. Mizuno, E.G. Nelson, Y. V. Sevryugina, *Angew. Chem. Int. Ed.* 54 (2015) 7900-7904.
- [23] L.R. Parent, Y. Cheng, P.V. Sushko, Y. Shao, J. Liu, C.-M. Wang, N.D. Browning, *Nano Lett.* 15 (2015) 1177-1182.
- [24] Y. Shao, M. Gu, X. Li, Z. Nie, P. Zuo, G. Li, T. Liu, J. Xiao, Y. Cheng, C. Wang, J.-G. Zhang, J. Liu, *Nano Lett.* 14 (2014) 255-260.
- [25] Y. Liang, H.D. Yoo, Y. Li, J. Shuai, H.A. Calderon, F.C. Robles Hernandez, L.C. Grabow, Y. Yao, *Nano Lett.* 15 (2015) 2194-2202.
- [26] Y. Liang, R. Feng, S. Yang, H. Ma, J. Liang, J. Chen, *Adv. Mater.* 23 (2011) 640.
- [27] Q.Y. An, P.F. Zhang, Q.L. Wei, L. He, F.Y. Xiong, J.Z. Sheng, Q. Q. Wang, L.Q. Mai, *J. Mater. Chem. A* 2 (2014) 3297-3302.
- [28] M.S. Whittingham, *Chem. Rev.* 104 (2004) 4271-4302.
- [29] P. Novak, J. Desilvestro, *J. Electrochem. Soc.* 140 (1993) 140-144.
- [30] P. Novak, W. Scheifele, F. Joho, O. Haas, *J. Electrochem. Soc.* 142 (1995) 2544-2550.
- [31] S.H. Lee, R.A. DiLeo, A.C. Marschilok, K.J. Takeuchi, E. S. Takeuchi, *Ecs Electrochem. Lett.* 3 (2014) 87-90.
- [32] G. Gershinsky, H.D. Yoo, Y. Gofer, D. Aurbach, *Langmuir* 29 (2013) 10964-10972.
- [33] B.G. Choi, M. Yang, W.H. Hong, J.W. Choi, Y.S. Huh, *Acs Nano* 6 (2012) 4020-4028.
- [34] J. Livage, *Chem. Mater.* 3 (1991) 578-593.
- [35] V. Petkov, P.N. Trikalitis, E.S. Bozin, S.J.L. Billinge, T. Vogt, M. G. Kanatzidis, *J. Am. Chem. Soc.* 124 (2002) 10157-10162.
- [36] F. Zhang, T.F. Zhang, X. Yang, L. Zhang, K. Leng, Y. Huang, Y. S. Chen, *Energy Environ. Sci.* 6 (2013) 1623-1632.
- [37] G.M. Zhou, L. Li, C.Q. Ma, S.G. Wang, Y. Shi, N. Koratkar, W. C. Ren, F. Li, H.M. Cheng, *Nano Energy* 11 (2015) 356-365.
- [38] W. Weppner, R.A. Huggins, *J. Electrochem. Soc.* 124 (1977) 1569-1578.
- [39] E. Deiss, *Electrochim. Acta* 50 (2005) 2927-2932.
- [40] M.D. Levi, E. Lancry, H. Gizbar, Y. Gofer, E. Levi, D. Aurbach, *Electrochim. Acta* 49 (2004) 3201-3209.
- [41] J. Song, L. Wang, Y.H. Lu, J. Liu, B.K. Guo, P.H. Xiao, J.J. Lee, X.Q. Yang, G. Henkelman, J.B. Goodenough, *J. Am. Chem. Soc.* 137 (2015) 2658-2664.



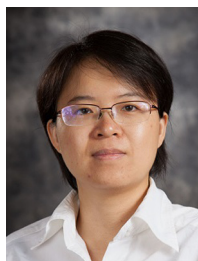
Qinyou An received his Ph.D. in Wuhan University of Technology in 2014. He is a postdoctoral fellow at the University of Houston with research interests on Mg-ion batteries.



Yifei Li received his B.S. degree from Wuhan University in 2012. He is currently pursuing a Ph.D. in Materials Science and Engineering at the University of Houston in Dr. Yan Yao's group. His research focuses on nanostructured electrode materials for advanced Na-ion and Mg-ion batteries.



**Hyun Deog Yoo** received Ph.D. in Chemical and Biological Engineering from Seoul National University in 2011, and then worked as a postdoctoral researcher in Prof. D. Aurbach's lab at Bar-Ilan University from 2011 to 2013. Since 2013, he joined Dr. Yan Yao's group at University of Houston as a postdoctoral researcher. His research interest is the electrochemistry of energy-storing materials including magnesium ion batteries and supercapacitors.



**Shuo Chen** is currently an assistant professor in the Department of Physics at the University of Houston. She earned her BS degree in Physics at Peking University, China and a Ph.D. degree from the Department of Physics at Boston College. Her research interests cover the material/device fabrication for clean/green energy application purposes and in situ Transmission Electron Microscopy.



**Qiang Ru** is an associate professor in South China Normal University and a visiting scholar at University of Houston. He received his Ph.D. in Guangdong University of Technology. His research interests are Mg-ion batteries for large-scale energy storage.



**Liqiang Mai** is Chair Professor of Materials Science and Engineering at Wuhan University of Technology (WUT) and Executive Dean of International School of Materials Science and Engineering at WUT. He received his Ph.D. from WUT in 2004. He carried out his postdoctoral research in the laboratory of Prof. Zhonglin Wang at Georgia Institute of Technology in 2006-2007 and worked as advanced research scholar in the laboratory of Prof. Charles M. Lieber at Harvard University in 2008-2011. His current research interests focus on nanowire materials and devices for energy storage. He received the National Natural Science Fund for Distinguished Young Scholars, the First Prize for Hubei Natural Science Award, etc.



**Yan Yao** received his B.S. and M.S. degrees in Materials Science from Fudan University in 2000 and 2003. He received his Ph.D. in Materials Science and Engineering at University of California, Los Angeles in 2008. He went on working as a senior scientist at Polyera Corporation and then as a postdoctoral fellow at Stanford University. In 2012, he joined the University of Houston as an assistant professor. His research interests focus on magnesium/sodium ion batteries, aqueous batteries, and organic materials for energy storage. He has received the ONR Young Investigator Award (2013), Ralph E. Powe Junior Faculty Enhancement Award (2013) and Robert A. Welch Professorship (2012).